Journal of Molecular Neuroscience (2018) 64:352–362
https://doi.org/10.1007/s12031-018-1030-5

Iron Oxide Nanoparticles Induces Cell Cycle-Dependent Neuronal Apoptosis in Mice

Vijayprakash Manickam[1] · Vasanth Dhakshinamoorthy[1] · Ekambaram Perumal[1]

Received: 1 December 2017 / Accepted: 11 January 2018 / Published online: 24 January 2018

Abstract

Iron oxide (Fe_2O_3) nanoparticles (NPs) with its unique magnetic and paramagnetic properties are popular in biomedical applications. Some of their neurotoxic mechanisms due to repeated administration are proven. However, we speculate that the neuronal damage might be due to apoptosis resulting from unusual cell cycle entry. Moreover, iron accumulation has been shown to be closely associated with most of the neurodegenerative disorders. Thus, in the current study, mice were orally (po) treated with the Fe_2O_3-NPs to investigate cell cycle-associated events/components and occurrence of apoptosis. A subsequent increase in oxidant levels was observed with the iron accumulation due to Fe_2O_3-NPs exposure. The accumulated β-amyloid and reduced level of cdk5 seem to aid in the cell cycle entry and forcing progression towards apoptosis. Expression of Cyclin D1 and pRb (Ser 795) indicate the cell cycle re-entry of neurons. Overexpression of RNA Pol II and PARP cleavage suggests DNA damage due to Fe_2O_3-NPs exposure. Further, hyperphosphorylation of p38 (Thr 180/Tyr 182) confirms the activation of DNA damage-dependent checkpoint. Expression patterns of pro- and anti-apoptotic markers, TUNEL and TEM indicate the occurrences of apoptosis.

Keywords Iron oxide NPs · Cell cycle · Apoptosis · β-amyloid · Oxidative stress

Introduction

Metal oxide nanoparticles (NPs) are widely used in biomedical science during recent years because of its coordinating environment of surface atoms, redox properties, and oxidative stat at their surface layers (Busca 2006). Iron oxide NPs such as Fe_3O_4 and Fe_2O_3 are considered superior to other metal oxide NPs due to their biocompatibility and stability. Further, Fe_2O_3-NPs have gained a greater importance in biomedical applications especially in neurotheranostics due to their advantageous physico-chemical properties such as size, charge, and electromagnetism (Mahmoudi et al. 2011). Fe_2O_3-NPs are also used in a number of other clinical applications including magnetic resonance imaging (MRI), targeted drug and gene delivery, tissue engineering, cell tracking, hyperthermia, magnetofection, and bioseparation (Ito et al. 2005; Duguet et al. 2006). However, Fe_2O_3-NPs are not without risk and health effects, likely by the release of free iron and reactive oxygen species (ROS) generation (Vogel et al. 2016).

The consequences of iron toxicity are of a serious concern, due to the possibilities of repeated exposure and bioaccumulation. Fe_2O_3-NPs seem to be the major source of iron accumulation in biological systems during biomedical applications regardless of the routes of administration (Patil et al. 2015). Despite the tight protection by the blood-brain barrier, Fe_2O_3-NPs have the capability to traverse and accumulate in the brain, making them more promising in neuroimaging (Wang et al. 2007a, b). Since iron is a transition metal, it readily undergoes Fenton's reaction and generates free radicals. The brain is rich in lipid and utilizes around 70% of consumed oxygen and thus the most vulnerable organ to oxidative stress through lipid peroxidation. Neurons are terminally differentiated post-mitotic cells; they neither enter the cell cycle nor apoptosis. However, unusual cell cycle re-entry has been registered in several neurodegenerative disorders, including Alzheimer's disease (AD) (Kawauchi et al. 2013). Iron accumulation seems to be a crucial candidate in most of the neurodegenerative disorders (Hagemeier et al. 2012). We assume that excessive iron might play a key role in aiding the neuronal cells to re-enter the cell cycle. But, the knowledge on iron-mediated neuronal apoptosis is limited. Though the neurotoxicity of Fe_2O_3-NPs has been proved to result in oxidative stress-mediated apoptosis, the details are poorly understood.

✉ Ekambaram Perumal
ekas2009@buc.edu.in

[1] Molecular Toxicology Laboratory, Department of Biotechnology, Bharathiar University, Coimbatore, Tamil Nadu 641 046, India

Table 1 Iron content in the serum and brain regions of control and test animals

Serum/brain regions	Control	25 mg/kg Fe_2O_3-NPs	50 mg/kg Fe_2O_3-NPs
Serum	21.2 ± 1.1	29.1 ± 1.3*	39.5 ± 2.4*#
Frontal cortex	12.5 ± 0.9	18.8 ± 1.5*	21.3 ± 0.5*#
Hippocampus	11.7 ± 0.7	14.7 ± 0.8*	19.5 ± 1.1*#
Cerebellum	11.3 ± 1.1	16.1 ± 2.3*	23.2 ± 2.3*#

Unit: microgram/deciliter serum and microgram/gram wet tissue. Values are mean ± SD of five animals in each group

*p<0.05 significantly different from control; #p<0.05 significantly different from 25 mg/kg Fe_2O_3-NPs treated mice (one-way ANOVA followed by Tukey's multiple comparison test).

The current study aims at exploring the series of facts involved in iron oxide-mediated neuronal apoptosis. On this pursuit, ultra-sonicated suspension of Fe_2O_3-NPs at the dose of 25 and 50 mg/kg was administered to male albino mice orally (po) for 30 consecutive days and focused on ROS, β-amyloid, cell cycle markers, and DNA damage, which are shown to be closely associated with apoptosis. This investigation reveals that Fe_2O_3-NPs augments β-amyloid accumulation and alters the expression of Cdk5 paving way for cell cycle re-entry. The ROS-mediated DNA damages activate the MAPK pathway, confirming the activation of the cell cycle check point. Further, TUNEL assay, TEM analysis of brain regions, and apoptotic markers confirm the occurrence of apoptosis. This study compiles that Fe_2O_3-NPs induces neuronal apoptosis via cell cycle re-entry.

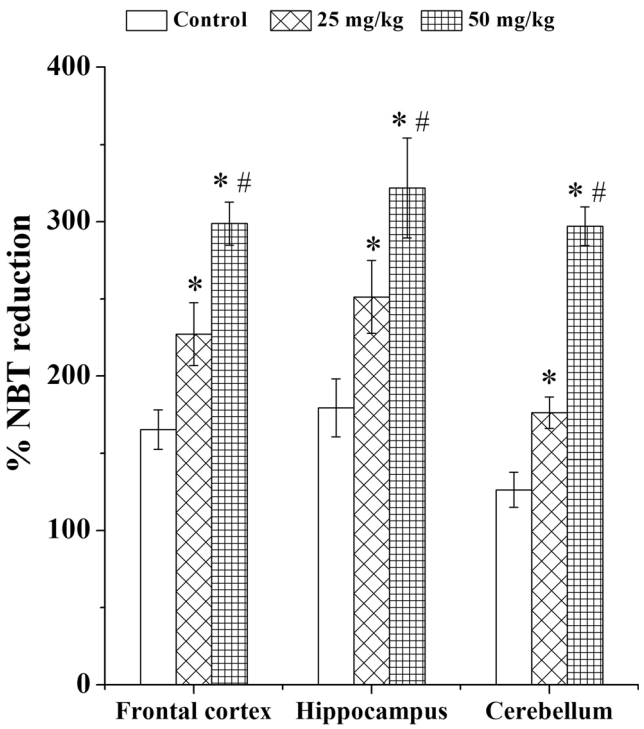

Fig. 1 Exposure to Fe_2O_3-NPs generates ROS in the mice brain regions. Values are mean ± SD of five animals in each group. *p<0.05 significantly different from control; #p<0.05 significantly different from 25 mg/kg Fe_2O_3-NPs treated mice (one-way ANOVA followed by Tukey's multiple comparison test)

Materials and Methods

Animals and Experimental Design

Male Swiss Albino mice (*Mus musculus*) were maintained under standard laboratory conditions and fed with pelleted mice chow (Sai Durga Feeds Pvt. Ltd., Bangalore, India); tap water was available ad libitum. All the experiments were conducted in accordance with the ethical norms approved by Institutional Animal Ethical Committee (722/02/A/CPCSEA). Fe_2O_3-NPs (< 50 nm) used throughout this study were purchased from Sigma-Aldrich (Cat#544884), and the average size, crystalline nature, charge, stability, and energy dispersion were analyzed (Dhakshinamoorthy et al. 2017; Sundarraj et al. 2017).

The NPs suspension was prepared freshly for every use by dispersing in 0.9% physiological saline followed by ultra-sonication. Eight-week-old animals weighing 25 to 30 g were randomly divided into three groups (n = 5 per group). Test animals were administered with Fe_2O_3-NPs suspension at the dose of 25 and 50 mg/kg orally (po) for 30 consecutive days while control animals received same volume of 0.9% physiological saline. The doses were chosen based on exposure range of Fe_2O_3-NPs in biomedical applications (Winer et al. 2012) and our pervious study (Sundarraj et al. 2017). After 24 h of the last treatment, animals were sacrificed by cervical decapitation and serum was separated. The brain was isolated and washed with 0.9% saline. The brain regions viz. frontal cortex, hippocampus, and cerebellum were carefully microdissected and used in further analysis. Different set of animals were used for each biochemical assay and molecular experiments.

Metal Analysis

The elemental analysis was done as described by Wang et al. (2007a, b). Briefly, about 25 mg of brain tissues and 50 μl of serum were digested with 0.5 ml of nitric acid (HNO_3). The mixture was incubated at 160 °C until complete digestion and the remaining HNO_3 was removed by heating at 120 °C. The final volume was made up to 3 ml using 2% HNO_3. Blank was prepared without the addition of sample. The concentration of Fe^{2+} in the serum and brain regions (frontal cortex, hippocampus, cerebellum) were measured by inductively coupled plasma mass spectrometry (ICP-MS) and expressed as

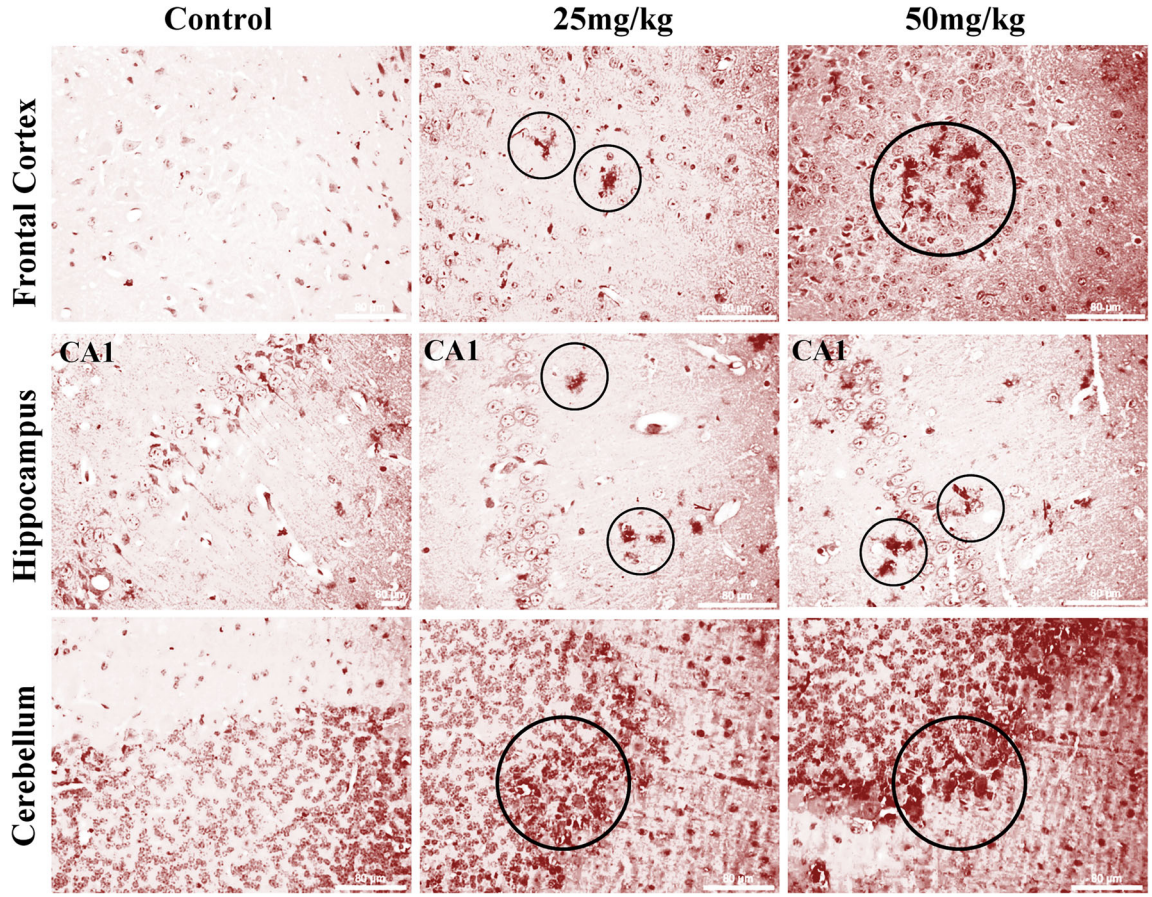

Fig. 2 Congo red staining for β-amyloid accumulation in the brain regions of control and Fe_2O_3-NPs treated mice (circle represents the β-amyloid accumulation)

microgram per gram and microgram per deciliter in wet tissue and serum, respectively.

ROS

ROS was measured by the nitroso blue tetrazolium (NBT) reduction method (Beauchamp and Fridovich 1971). Nitroblue tetrazolium reduction is used as an indicator for superoxide production. The principle of this assay is based upon the ability of superoxide to interact with NBT, reducing the yellow tetraxolium to blue color precipitate (NBTH). Thus, the superoxide generated by an oxidase-catalyzed reaction can be assayed by degree of NBT reduction. Ten milligrams of tissue was taken in 1 ml of Hank's balance salt solution and homogenized. To the test sample, 0.5 ml of NBT-HBSS was added and incubated at 37 °C for 8 h. After incubation, the test samples were centrifuged at 1000 rpm for 10 min at 4 °C. The pellets were washed thrice with 200 μl of methanol. Following this, the pellets were dissolved in 1 ml of 2 M KOH and 1 ml of DMSO and the OD values were observed at 630 nm. The readings were compared with the standard curve constructed with NBT. ROS generation is expressed as percentage of NBT reduced.

Western Blotting

To examine the expression of β-amyloid, cell cycle proteins, and apoptotic markers, Western blotting analysis was performed as described previously (Dhakshinamoorthy et al. 2017). Each excised membrane was incubated individually with goat anti-β-amyloid (1:2500), rabbit anti-Cdk5 (1:2500), mouse anti-cyclin D1 (1:1000), rabbit anti-Rb (1:1000) and goat anti-p-Rb (Ser 795) (1:1000), rabbit anti-p38 (1:2500), rabbit anti-p-p38 (Thr180/Try182) (1:1000), mouse anti-RNA Pol II (1:2500), rabbit anti-PARP (1:2500), mouse anti-Bax (1:1000), rabbit anti-Bcl-2 (1:1000), mouse anti-caspase 3 (1:1000), and mouse anti-β-actin (1:5000).

The proteins were detected using horseradish peroxidase (HRP)-conjugated anti-rabbit, anti-goat, or anti-mouse secondary antibodies (1:2500) and visualized by 3, 3′-diaminobenzidine (DAB) staining (0.02% DAB in 0.01% H_2O_2). The same procedure was followed for hippocampus and cerebellum lysates. β-actin was used as the internal control to ensure equal sample loading and western transfer. Densitometry analyses of immuno blots were quantified using the *ImageJ* analysis software from the National Institute of Health (NIH).

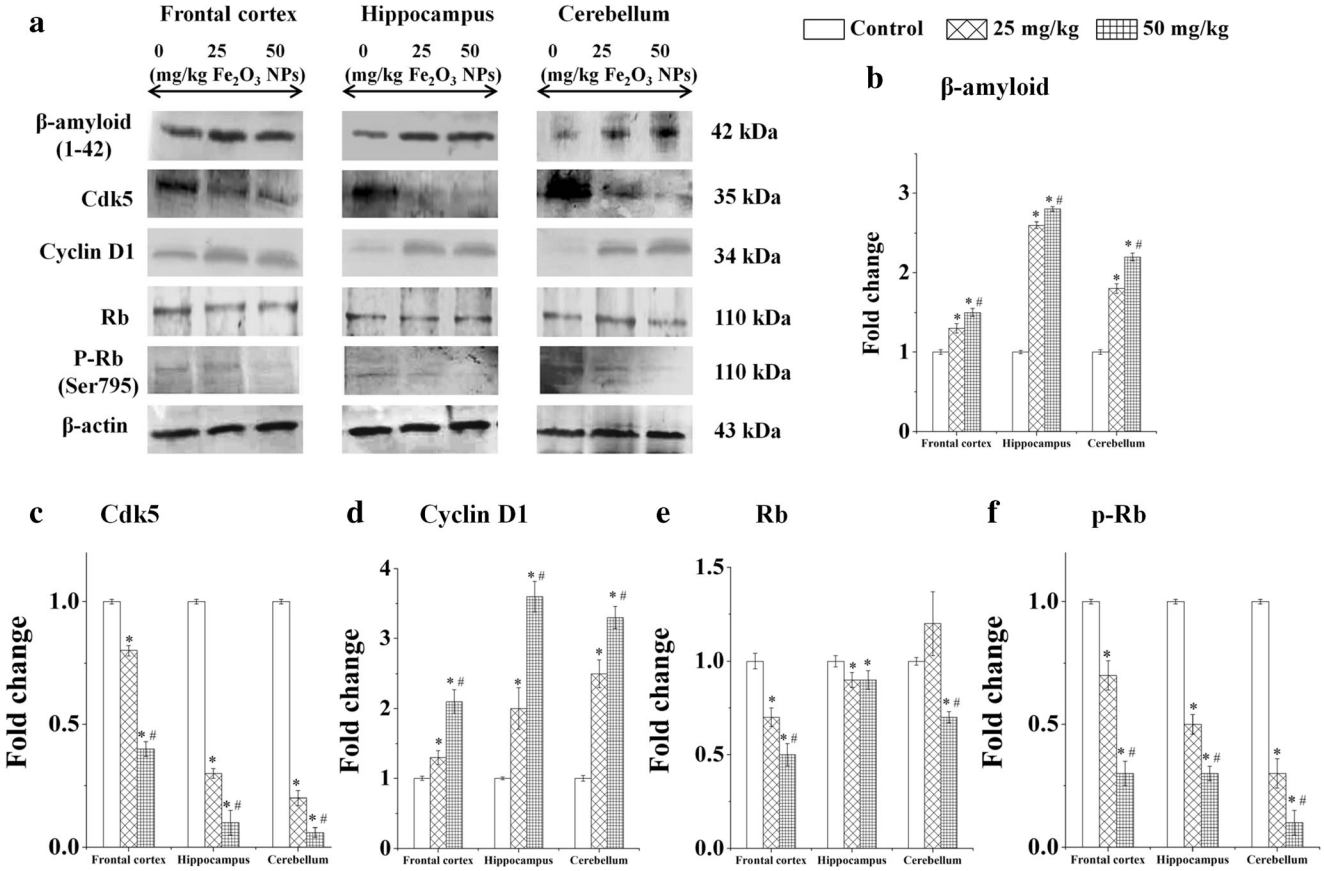

Fig. 3 Exposure to Fe_2O_3-NPs induces neuronal cell cycle. **a** Western blot shows the expression pattern of β-amyloid and Cdk5, the stress response, and cell cycle regulator proteins respectively in neurons. Increased Cyclin D1 and expression pattern of total Rb and p-Rb (Ser 795) confirm the cell cycle events. **b–f** Corresponding densitometry analysis. Values are mean ± SD of three animals in each group. *$p<0.05$ significantly different from control; #$p<0.05$ significantly different from 25 mg/kg Fe_2O_3-NPs treated mice (one-way ANOVA followed by Tukey's multiple comparison test)

Congo Red Staining

Deposition of β-amyloid was observed using modified Highman's congo red stains (Kulkarni et al. 2010). Tissue sections of 5 μm were prepared. Sections were deparaffinized and hydrated to water using decreasing concentration of alcohol. The sections were incubated with congo red stain (0.5% congo red in 50% alcohol) for 15 min at room temperature. The slides were dehydrated using alcohol and mounted with distrene plasticizer xylene. The sections were observed under the microscope.

Terminal Deoxynucleotidyl Transferase (TdT) -Mediated Biotin-dUTP Nick End Labelling (TUNEL) Assay

TUNEL assay was performed using an in situ apoptosis detection kit (Roche Applied Science, Penzberg, Upper Bavaria, Germany). The paraffin-embedded brain tissue of unstained sections with 5 μ thickness of the frontal cortex, hippocampus, and cerebellum was prepared from the control and Fe_2O_3-NPs-treated mice. The sections were deparaffinized in fresh xylene at 60 °C for 20 min and dehydrated with the different grade of ethanol solution. The tissue sections were pre-treated with 20 μg/ml of proteinase K solution prepared in 10 mM Tris/HCL, pH 7.4–8.0, *w/v* for 10 min to avoid false-positive results. After washing with PBS solution, the sections were incubated with TUNEL reaction mixture for 1 h at 37 °C in the humidified chamber at the dark condition. Finally, the sections were washed with PBS and incubated with 4′, 6-diamidino-2-phenylindole (DAPI) (Sigma-Aldrich, St. Louis, USA) for 8 min in the dark at room temperature and examined with the fluorescence microscope (Olympus, Japan) under ×400 magnifications. Relative cell death was calculated by counting TUNEL-positive nuclei and total DAPI-stained nuclei in the tissue.

Ultra-Structural Analysis of Brain Regions

After treatment, the animals were subjected to vascular perfusion with the mixture of 2.5% glutaraldehyde and

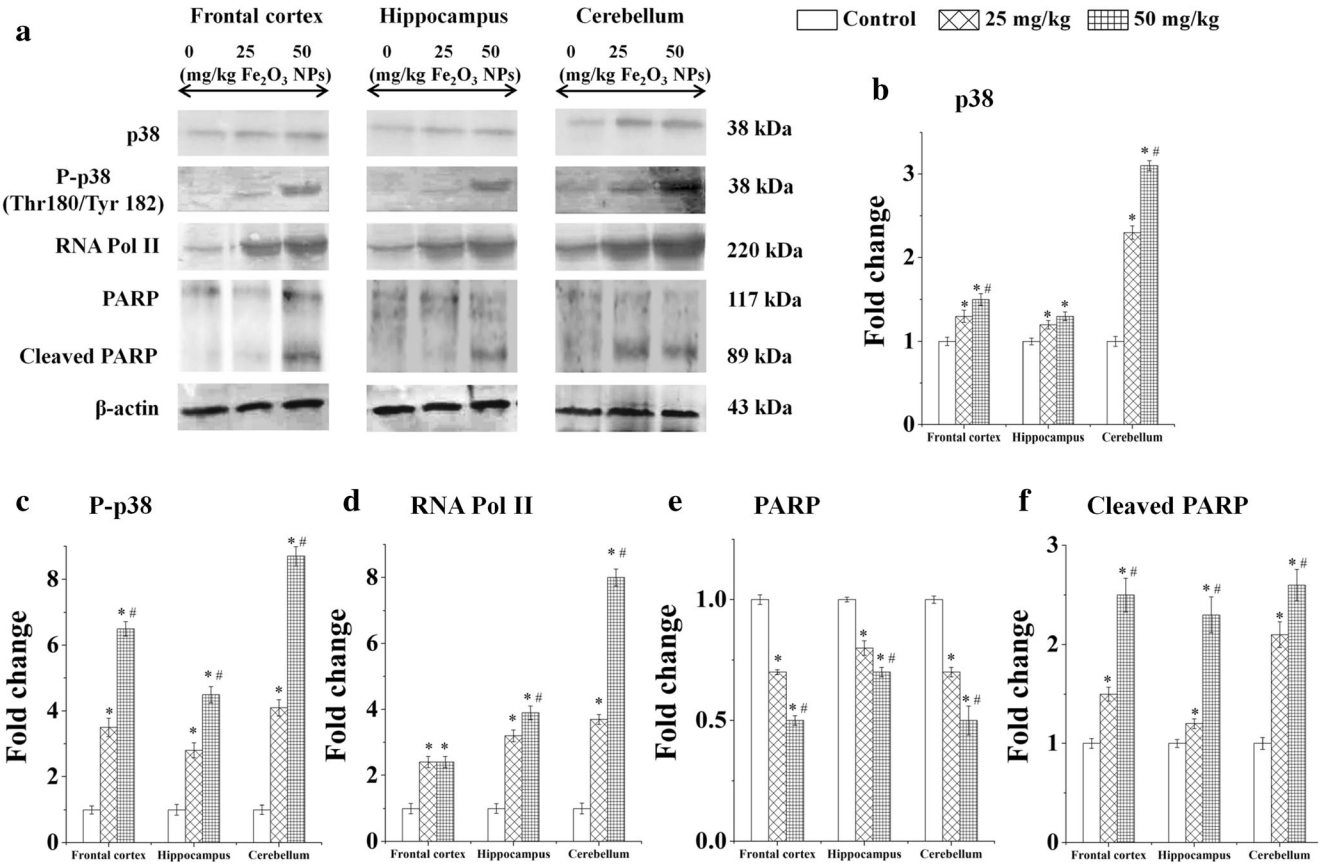

Fig. 4 Fe_2O_3-NPs damages DNA and activates cell cycle check point. **a** Western blot shows the expression pattern of DNA damage markers RNA Pol II and PARP. The expression of total p38 and p38 (Thr 180/Tyr 182) indicates the activation of G1/S checkpoint through the MAPK pathway. **b–f** Corresponding densitometry analysis. Values are mean ± SD of three animals in each group. *p<0.05 significantly different from control; #p<0.05 significantly different from 25 mg/kg Fe_2O_3-NPs treated mice (one-way ANOVA followed by Tukey's multiple comparison test)

2% paraformaldehyde, made in 0.1 M sodium phosphate buffer (pH 7.4). The brain regions were fixed with the same fixative at 4 °C. After fixation, about 2 mm of respective brain regions were excised and further trimmed into 1 mm pieces. The tissues were osmicated, dehydrated, and embedded in araldite CY212. The area from 500 nm block was selected using the light microscope after staining with 0.5% toluidine blue. The blocks were cut by using ultra-microtome contrasted with uranyl acetate and lead citrate and observed under TECANI G20 transmission electron microscope (FEI Company, Netherland).

Statistical Analysis

All the values were expressed as mean ± SD of five animals in each group. The data were analyzed with one-way analysis of variance (ANOVA) followed by Tukey's multiple comparison tests using the SPSS (20.0) software package. $p < 0.05$ was considered to indicate statistical significance.

Results

Exposure to Fe_2O_3-NPs Increases the Bioaccumulation of Iron

The iron content in the serum and brain regions of test animals was found to be significantly increased in a dose-dependent manner when compared with the control (Table 1).

Exposure to Fe_2O_3-NPs Increases the Oxidant Levels

Dose-dependent increase in ROS was observed in the brain regions of treated groups as compared to the control (Fig. 1).

Fe_2O_3-NPs Induces β-Amyloid Accumulation

A significant increase in the expression of β-amyloid was evidenced in the brain regions of Fe_2O_3-NPs-exposed groups compared to control. The congo red light up the neuritic plaques (senile plaques) due to β-amyloid accumulation (Fig. 2). The degree of red staining is very less in the brain regions of the control animals. The treated brain regions show

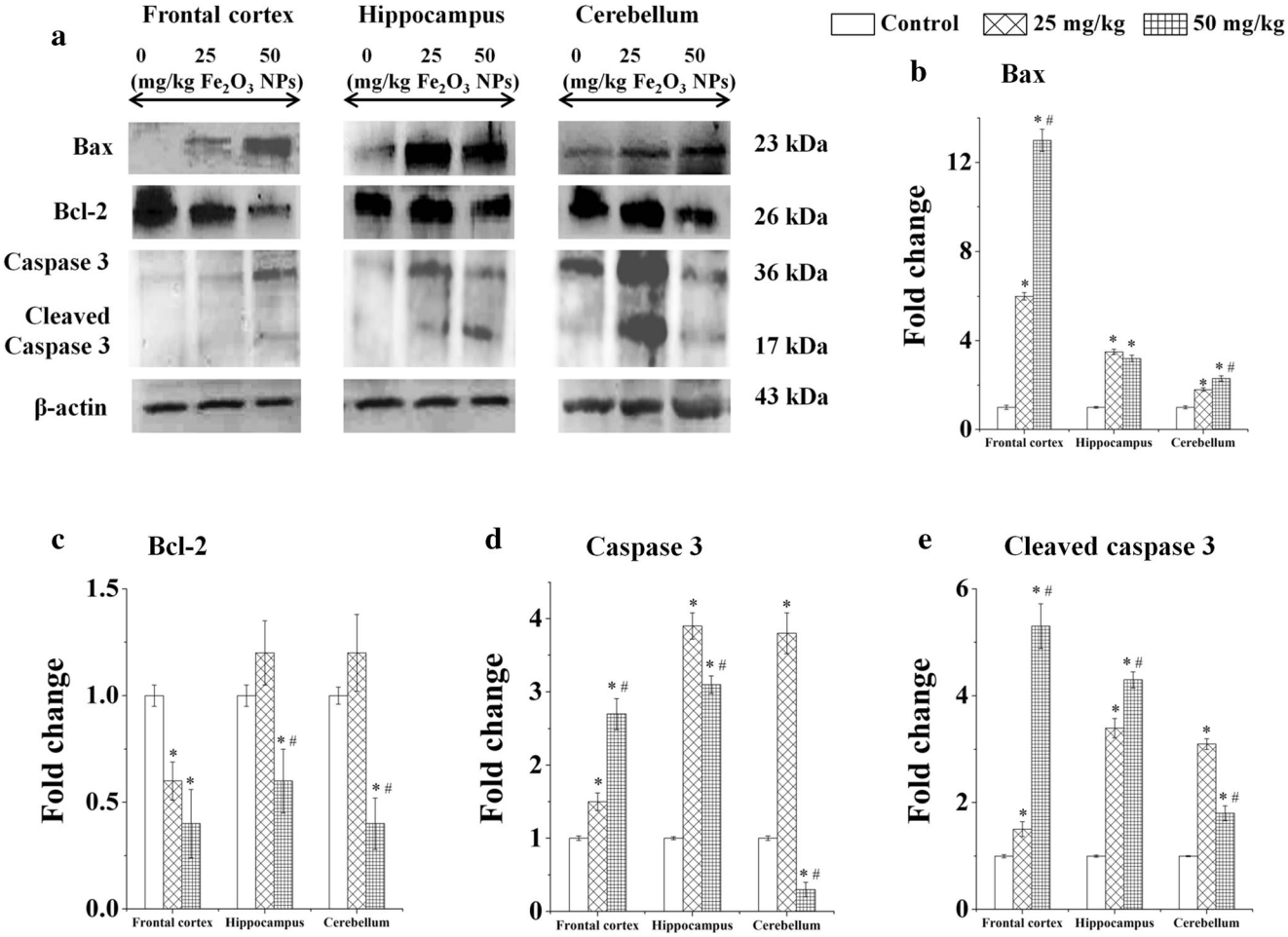

Fig. 5 Fe_2O_3-NPs induces apoptosis. **a** Western blot reveals the expression pattern of pro-apoptotic (Bax and cleaved Caspase) and anti-apoptotic (Bcl-2) markers in the brain regions of control and intoxicated animals. **b–e** Corresponding densitometry analysis. Values are mean ± SD of three animals in each group. *p<0.05 significantly different from control; #p<0.05 significantly different from 25 mg/kg Fe_2O_3-NPs treated mice (one-way ANOVA followed by Tukey's multiple comparison test)

the increased levels of neuritic plaques. β-amyloid over expression was further confirmed by the Western blotting (Fig. 3). Significant overexpression of β-amyloid was observed in the brain regions of treated animals.

Fe_2O_3-NPs Promotes Neuronal Cell Cycle Re-Entry

Blotting results shows upregulation of cyclin D1 and downregulation of Rb in the brain regions of test animals (Fig. 3). Decreased level of Cdk5 was observed in brain regions of treated animals compared to controls. Subsequent increase in the Cyclin D1expression was also observed. Further, decreased levels of total Rb and p-Rb expression were observed in the treated animals.

Fe_2O_3-NPs Damages DNA

There was an increased expression of p38, P-p38 (Thr 180/Tyr 182), and RNA Pol II in the brain regions of treated animals compared to control. Dose-dependent decrease in the level of total PARP and simultaneous increase in the levels of cleaved PARP was observed in all the brain regions of Fe_2O_3-NPs-treated animals (Fig. 4).

Fe_2O_3-NPs Induces Neuronal Apoptosis

Pro-apoptotic protein (Bax) and apoptotic marker (cleaved caspase-3) were found to be increased in the brain regions in contrast to anti-apoptotic protein (Bcl-2) (Fig. 5). The frontal cortex shows a decrease in Bcl-2 levels. The hippocampus and cerebellum shows increased level of Bcl-2 in 25 mg/kg compared to control. However, it is not statistically significant. Fifty milligram/kilogram shows a significant decrease in Bcl-2 level. The frontal cortex and hippocampus shows the dose-dependent decreased levels of total caspase3 and increased level of cleaved caspase 3. In the cerebellum, 25 mg/kg shows the increased level of total caspase 3 compared to the control and 50 mg/kg. However, cleaved caspase3 level is found to be more in 25 mg/kg than in 50 mg/kg compared to control.

Increased TUNEL-positive cells were noted in the Fe_2O_3-NPs-treated brain regions compared with the

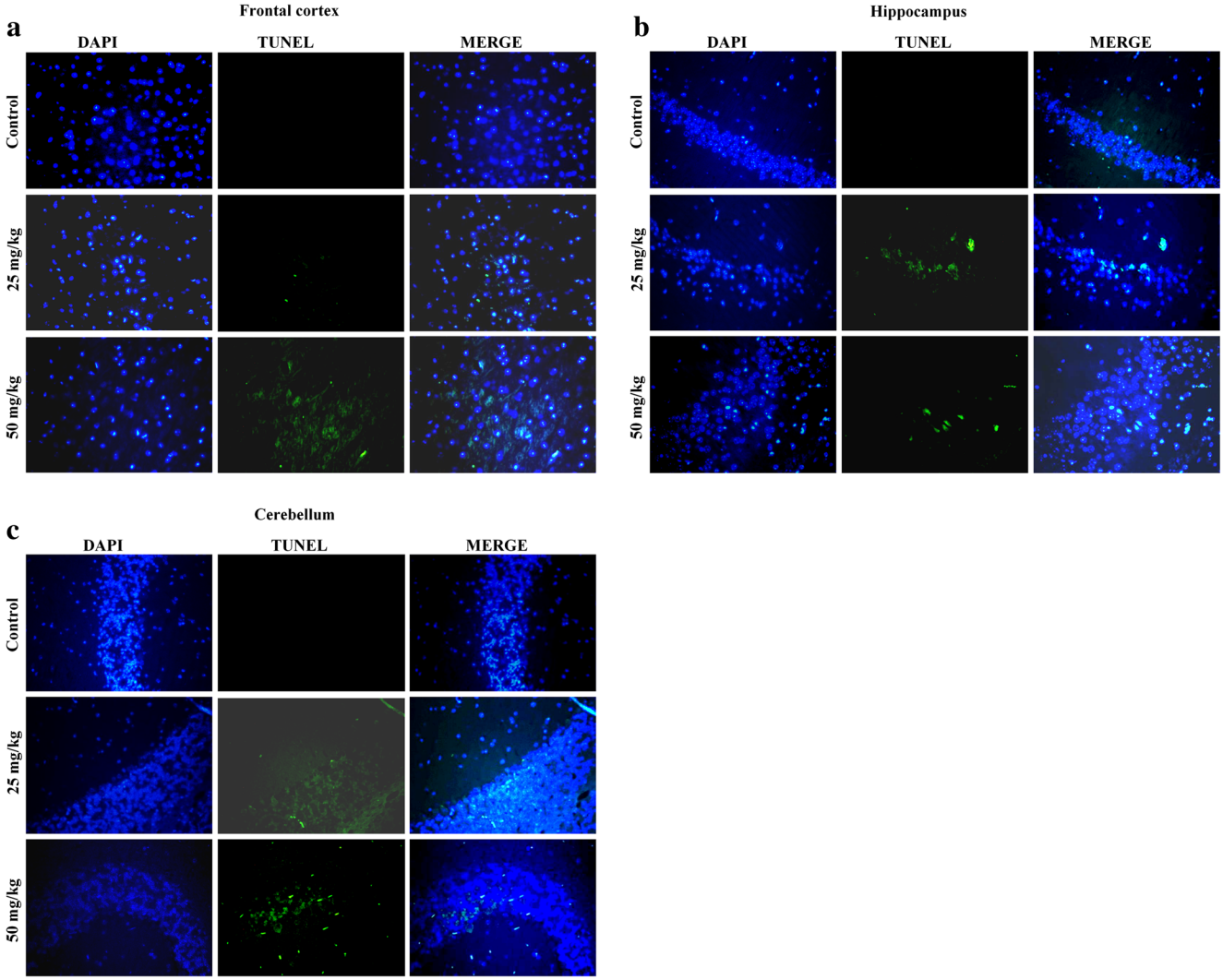

Fig. 6 Representative images of TUNEL analysis showing DNA damage and apoptosis in the **a** frontal cortex, **b** hippocampus, and **c** cerebellum of control and Fe_2O_3-NPs treated mice

control (Fig. 6a–c). TEM images reveal the damaged cell architecture of treated brain regions. The degree of cell damage is increased dose dependently. In the frontal cortex, the control animal shows the nucleus with normal nuclear content; whereas, the treated animals show the precipitated nuclear content attached to the nuclear envelope. In the hippocampus, there were unknown vacuoles disconnecting the nuclear and cytoplasmic communications. The cerebellum of the treated animal shows the extremely damaged cytoplasm and organelles (Fig. 7).

Discussion

Physico-chemical properties of Fe_2O_3-NPs were characterized which help us in data interpretation (Dhakshinamoorthy et al. 2017). The present study addresses the key events of Fe_2O_3-NPs-mediated neuronal cell cycle induction resulting in apoptosis. The free radical-rich environment due to iron accumulation forces post-mitotic neurons into the cell cycle, consequently to the apoptotic pathway. β-amyloid accumulation in the brain regions due to Fe_2O_3-NPs toxicity (Tahirbegi et al. 2016; Yarjanli et al. 2017) might be attributed to neuronal cell cycle re-entry (Li et al. 2008; Lopes et al. 2009; Wu et al. 2013). Properties of Fe_2O_3-NPs as a transition metal oxide and its tendency to damage biomolecules through ROS are well established (Dakshinamoorthy et al. 2017). Further, iron accumulation-mediated oxidative stress seems to aid the accumulation of β-amyloid in brain regions (Yarjanli et al. 2017).

Unusual re-entry of neurons into the cell cycle seems to be a hallmark in several neurodegenerative diseases including AD (Bonda et al. 2010), Parkinson's disease (Folch et al. 2012), and Huntington's disease (Akashiba et al. 2008; Pelegrí et al. 2008). The reasons behind the cell cycle re-entry by post-mitotic neurons are not clear, but apoptosis has been evidenced as the consequence

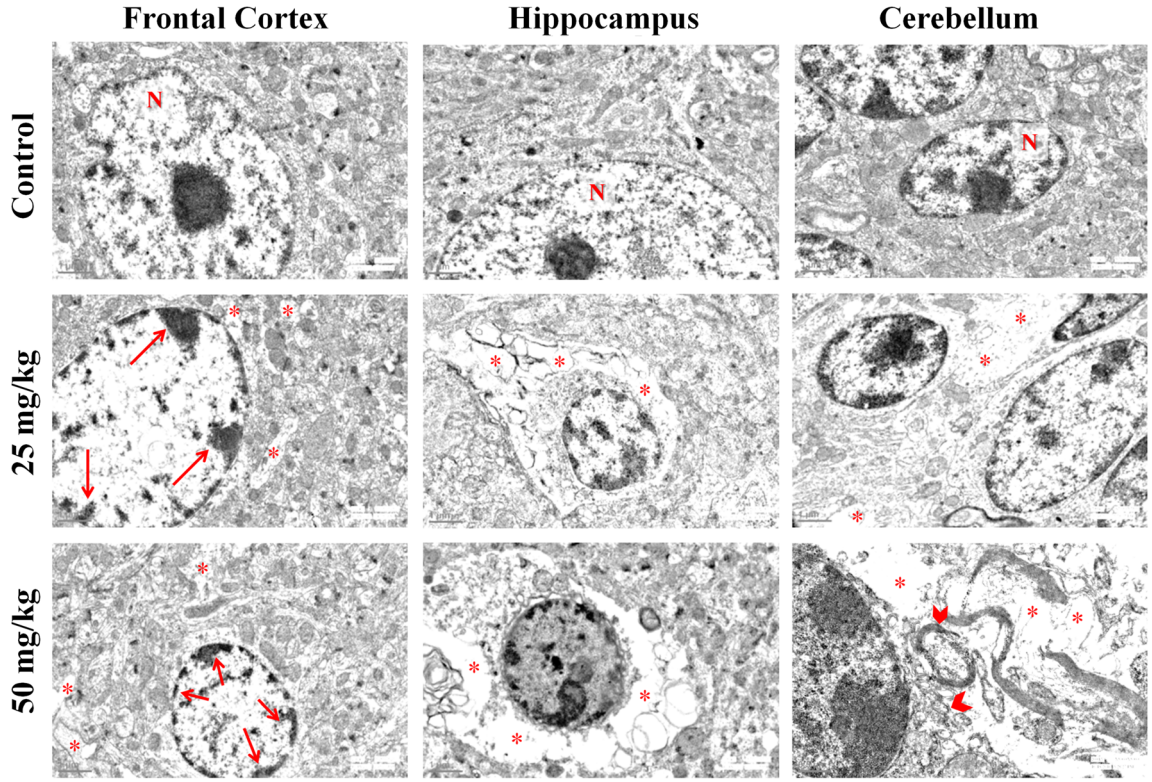

Fig. 7 Ultra-structural changes in the neurons due to Fe_2O_3-NPs. Control brain regions shows intact nucleus and nuclear material. Whereas, treated brain regions shows disintegrated nuclear material and precipitation of nuclear material on the nuclear membrane (arrow). Normal architecture of cytoplasm was observed in the neurons of control brain regions and treated group shows undefined vacuoles (star). Hippocampal neuron shows the loss of connectivity between the nucleus and cytoplasm by the formation of vacuoles indicating the early apoptosis. Cerebellum neurons of treated mice shows the cytoplasmic collapse and membrane disintegration (big arrow head) indicating the late apoptosis

because of their limited options (Meikrantz and Schlegel 1995; Wang et al. 2009).

During the stress condition, Cdk5, a neurospecific protein kinase, shuttles between the nucleus and cytoplasm, which plays a crucial role in preventing the cell cycle re-entry of the post-mitotic neurons (Zhang and Herrup 2008). When neurons enter the cell cycle, Cdk5 is momentarily translocated to the cytoplasm where it is rapidly degraded by proteosomes (Zhang et al. 2012). Cultured cortical neurons show Cdk5 dysregulations and abortive cell cycle re-entry when treated with β-amyloid and prion peptides (Lopes et al. 2009). Further, Cdk5 is majorly involved in the transition of G0 to G1 phase prior to Rb phosphorylation. Nevertheless, the exact role and the final target of Cdk5 in G0 to G1 transition remain elusive (Lopes et al. 2009). Neuronal cell cycle re-entry might be attributed to reduction in Cdk5 expression, observed in the present study. Thus, β-amyloid accumulation due to prolonged exposure to Fe_2O_3-NPs might have suppressed Cdk5 (Czapski et al. 2011).

Cyclin D1 is a key protein in cell cycle progression (Modi et al. 2016) and also an important G0/G1 transition marker (McShea 2007; Zhu 2007). Retinoblastoma protein (Rb) is a tumor suppressor protein (Genovese et al. 2006) that maintains the differentiated nature of neurons (Naser et al. 2016, Lee et al. 1994) in addition to its crucial role in G1 to S phase transition (Stone et al. 2011). Rb is shown to be hyper-phosphorylated at the early G1 phase at Ser 795 position by cyclin D1 for transition into the S phase (Guo et al. 2005). On the contrary, we observed dose-dependent decrease in the expression of phosphorylated Rb in the test animals suggesting the occurrence of apoptosis, since phosphorylated Rb is the substrate for cleaved caspase 3 (Pucci et al. 2000; Katsuda et al. 2002).

DNA damage by Fe_2O_3-NPs through ROS generation is well documented (Dissanayake et al. 2015). Evidence shows the activation of the neuronal cell cycle in the differentiated neurons before cell death (Schwartz et al. 2007). As DNA is the major target of the oxyradicals, cell cycle-associated events are the critical consequences of DNA damage response in the cycling cells. Studies have shown the same mechanisms in quiescent cells like neurons to undergo the repair mechanisms in possible cases or initiate the apoptosis during extensive damages (Kruman 2004). In the current study, overexpression of RNA Pol II (Bregman et al. 2000) and cleavage of PARP clearly indicate the DNA damage, aborting the cell cycle. Cleaved PARP in response to DNA damage activates p38-α, a protein responsible for cell cycle regulation, survival, and apoptosis (Thornton and Rincon 2009) involving the

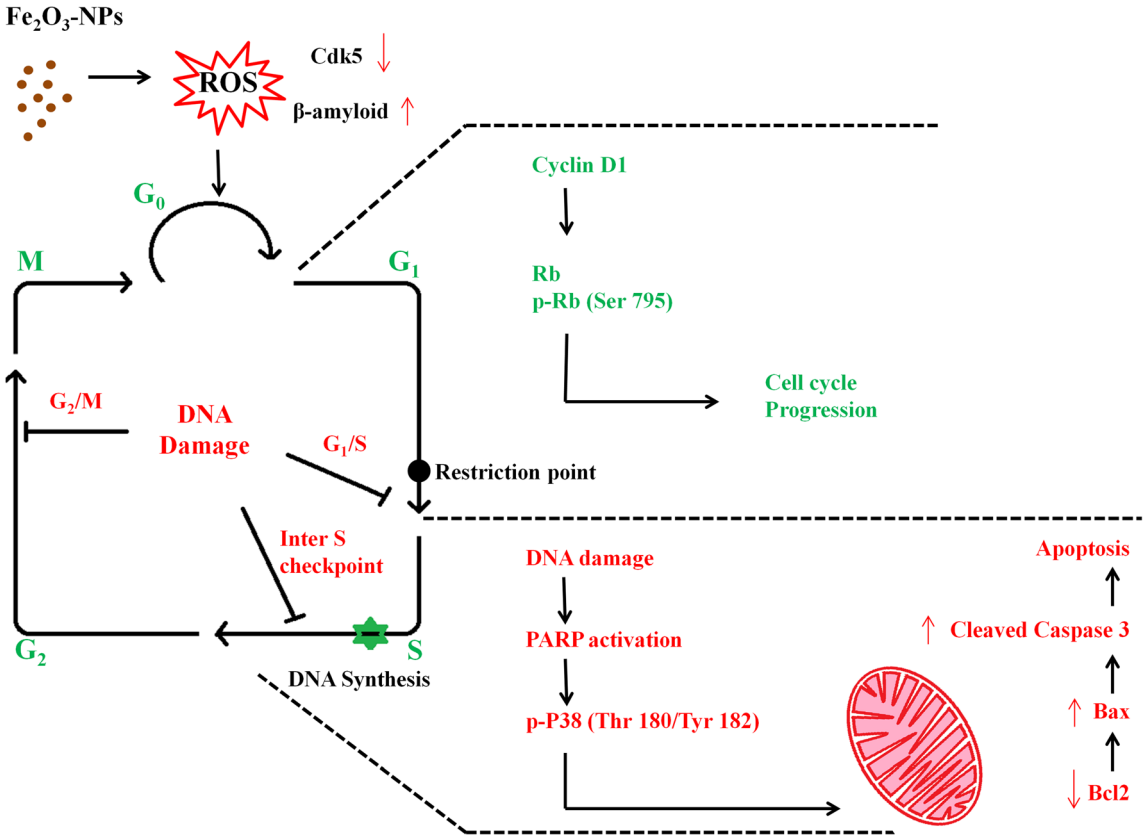

Fig. 8 Schematic representation of cell cycle-mediated neuronal apoptosis by Fe_2O_3-NPs. Post-mitotic status of neurons are majorly regulated by Cdk5. Decreased Cdk5 levels and increased β-amyloid accumulation makes post-mitotic neurons to re-enter into the cell cycle. Overexpression of Cyclin D1, an important cell cycle initiating protein, activates Rb. Thus, the release of E2F factor leads to the transcription of S phase proteins. On the other hand, excessive DNA damages leads to the activation of PARP and p38 (Thr 180/Tyr 182). Active p38 consequently leads to the mitochondrial-mediated apoptosis

MAP kinase pathway. This non-canonical phosphorylation of p38 (Thr 180/Tyr 182) is a hallmark of G1 to S phase checkpoint activation (Cuenda and Rousseau 2007; Joaquin et al. 2012).

Under the conditions like deprivation of neurotrophic factors, oxidative stress, DNA damage, and excitotoxicity, there occurs neuronal cell death at G1 to S checkpoint before entering into the synthesis phase of the cell cycle (Frade and Benito 2015). This is classically referred as "abortive cell cycle re-entry" which is characterized by the upregulation of cell cycle and apoptotic proteins (Park et al. 2000; Chen et al. 2013). Apoptosis observed through TUNEL assay of treated brain regions indicate that Fe_2O_3-NPs triggers abortive cell cycle re-entry.

The expression patterns of apoptosis regulatory proteins in the present investigation evident the occurrence of apoptosis. Activated p38 influence the mitochondrial damage by downregulating Bcl2, an anti-apoptotic protein and upregulating Bax, a pro-apoptotic protein (Tyagi and Herr 2009). Though apoptosis is recorded as the major mechanism of cell death of nanotoxicity (Fu et al. 2014), the expression pattern of caspase 3 in the cerebellum suggests the occurrences of other cell death mechanisms at higher doses (Manickam et al. 2017). TEM images of Fe_2O_3-NPs-exposed brain regions shows ultra-structural changes such as disintegrated nuclear material, undefined vacuoles, and organelle membrane damages, confirming the early and late apoptosis. Figure 8 shows the schematic representation of the current study.

In conclusion, the oxidative stress generated by Fe_2O_3-NPs potentially damages biomolecules. Fe_2O_3-NPs exposure induces neuronal apoptosis through an unusual cell cycle re-entry manipulating the cell cycle regulatory protein Cdk 5 and β-amyloid accumulation. The present study shows a clear link between cell cycle regulation, DNA damage, repair, and apoptosis due to neurotoxicity of NPs. However, further molecular studies are recommended to substantiate the current finding since the clinical applications of Fe_2O_3-NPs is on the rise.

Acknowledgements The authors would like to acknowledge Sophisticated Analytical Instrument Facility, All India Institute of Medical science (AIIMS), New Delhi, for the technical assistance in transmission electron microscopy. Vijayprakash Manickam acknowledges the UGC-BSR fellowship (UGC-BSR-No.F.7-25/2007) funded by UGC-BSR, New Delhi, India. We also thank the UGC-SAP DRS II (F-3-30/2013) and DST FIST (SR/FST/LSI-618/2014), New Delhi, India, for their partial financial assistance.

Compliance with Ethical Standards All the experiments were conducted in accordance with the ethical norms approved by Institutional Animal Ethical Committee (722/02/A/CPCSEA).

Conflict of Interest The authors declare that they have no conflict of interest.

Ethical Approval All procedures performed in this study involving animals were in accordance with the ethical standards of the institution or practice at which the studies were conducted.

References

Akashiba H, Ikegaya Y, Nishiyama N, Matsuki N (2008) Differential involvement of cell cycle reactivation between striatal and cortical neurons in cell death induced by 3-nitropropionic acid. J Biol Chem 283(10):6594–6606. https://doi.org/10.1074/jbc.M707730200

Beauchamp C, Fridovich I (1971) Superoxide dismutase: improved assays and an assay applicable to acrylamide gels. Anal Biochem 44(1):276–287. https://doi.org/10.1016/0003-2697(71)90370-8

Bonda DJ, Bajic VP, Spremo-Potparevic B, Casadesus G, Zhu X, Smith MA, Lee HG (2010) Review: cell cycle aberrations and neurodegeneration. Neuropathol Appl Neurobiol 36(2):157–163. https://doi.org/10.1111/j.1365-2990.2010.01064.x

Bregman DB, Pestell RG, Kidd VJ (2000) Cell cycle regulation and RNA polymerase II. Front Biosci 5:244–257

Busca G (2006) The surface acidity and basicity of solid oxides and zeolites. In: Fierro JLG (ed) Metal oxides, chemistry and applications. CRC Press, pp 247–318

Chen MJ, Ng JM, Peng ZF, Manikandan J, Yap YW, Llanos RM, Beart PM, Cheung NS (2013) Gene profiling identifies commonalities in neuronal pathways in excitotoxicity: evidence favouring cell cycle re-activation in concert with oxidative stress. Neurochem Int 62(5):719–730. https://doi.org/10.1016/j.neuint.2012.12.015

Cuenda A, Rousseau S (2007) p38 MAP-kinases pathway regulation, function and role in human diseases. Biochim Biophys Acta 1773(8):1358–1375. https://doi.org/10.1016/j.bbamcr.2007.03.010

Czapski GA, Gąssowska M, Songin M, Radecka UD, Strosznajder JB (2011) Alterations of cyclin dependent kinase 5 expression and phosphorylation in amyloid precursor protein (APP) transfected PC12 cells. FEBS Lett 585(8):1243–1248. https://doi.org/10.1016/j.febslet.2011.03.058

Dhakshinamoorthy V, Manickam V, Perumal E (2017) Neurobehavioral toxicity of iron oxide nanoparticles in mice. Neurotox Res 32:187–203

Dissanayake NM, Current KM, Obare SO (2015) Mutagenic effects of iron oxide nanoparticles on biological cells. Int J Mol Sci 16(10):23482–23516. https://doi.org/10.3390/ijms161023482

Duguet E, Vasseur S, Mornet S, Devoisselle JM (2006) Magnetic nanoparticles and their applications in medicine. Nanomed 1(2):157–168. https://doi.org/10.2217/17435889.1.2.157

Folch J, Junyent F, Verdaguer E, Auladell C, Pizarro JG, Zarate CB, Pallas M, Camins A (2012) Role of cell cycle re-entry in neurons: a common apoptotic mechanism of neuronal cell death. Neurotox Res 22(3):195–207. https://doi.org/10.1007/s12640-011-9277-4

Frade JM, Benito MCO (2015) Neuronal cell cycle: the neuron itself and its circumstances. Cell Cycle 14(5):712–720. https://doi.org/10.1080/15384101.2015.1004937

Fu PP, Xia Q, Hwang H, Ray PC, Yu H (2014) Mechanisms of nanotoxicity: generation of reactive oxygen species. J Food Drug Anal 22(64–7):5

Genovese C, Trani D, Caputi M, Claudio Z (2006) Cell cycle control and beyond: emerging roles for the retinoblastoma gene family. Oncogene 25(38):5201–5209. https://doi.org/10.1038/sj.onc.1209652

Guo J, Sheng G, Warner BW (2005) EGF induced rapid Rb phosphorylation at Ser780 and Ser795 is mediated by ERK1/2 in small intestine epithelial cells. J Biol Chem 280(43):35992–35998. https://doi.org/10.1074/jbc.M504583200

Hagemeier J, Geurts JJ, Zivadinov R (2012) Brain iron accumulation in aging and neurodegenerative disorders. Expert Rev Neurother 12(12):1467–1480. https://doi.org/10.1586/ern.12.128

Ito A, Shinkai M, Honda H, Kobayashi T (2005) Medical application of functionalized magnetic nanoparticles. J Biosci Bioeng 100:1–11

Joaquin M, Gubern A, Posas F (2012) A novel G1 checkpoint mediated by the p57 CDK inhibitor and p38 SAPK promotes cell survival upon stress. Cell Cycle 11:3339–3350

Katsuda K, Kataoka M, Uno F, Murakami T, Kondo T, Roth JA, Tanaka N, Fujiwara T (2002) Activation of caspase-3 and cleavage of Rb are associated with p16-mediated apoptosis in human non-small cell lung cancer cells. Oncogene 21(13):2108–2123. https://doi.org/10.1038/sj.onc.1205272

Kawauchi S, Shikanai M, Kosodo Y (2013) Extra-cell cycle regulatory functions of cyclin-dependent kinases (CDK) and CDK inhibitor proteins contribute to brain development and neurological disorders. Genes Cells 18:176–194

Kruman II (2004) Why do neurons enters cell cycle. Cell Cycle 3(6):769–773

Kulkarni PV, Roney CA, Antich PP, Bonte FJ, Raghu AV, Aminabhavi TM (2010) Quinolinenbutylcyanoacrylate based nanoparticles for brain targeting for the diagnosis of Alzheimer's disease. Wiley Interdisciplinary Rev Nanomed Nanobiotechnol 2(1):35–47. https://doi.org/10.1002/wnan.59

Lee EY, Hu N, Yuan SS, Cox LA, Bradley A, Lee WH, Herrup K (1994) Dual roles of the retinoblastoma protein in cell cycle regulation and neuron differentiation. Genes Dev 8:21–36

Li JJ, Zou L, Hartono D, Ong CN, Bay BH, Yung LY (2008) Gold nanoparticles induce oxidative damage in lung fibroblasts in vitro. Adv Mater 20(1):138–142. https://doi.org/10.1002/adma.200701853

Lopes JP, Oliveira CR, Agostinho P (2009) Cdk5 acts as a mediator of neuronal cell cycle re-entry triggered by amyloid-β and prion peptides. Cell Cycle 8(1):97–104. https://doi.org/10.4161/cc.8.1.7506

Mahmoudi M, Laurent S, Shokrgozar MA, Hosseinkhani M (2011) Toxicity evaluations of superparamagnetic iron oxide nanoparticles: cell "vision" versus physicochemical properties of nanoparticles. ACS Nano 5(9):7263–7276. https://doi.org/10.1021/nn2021088

Manickam V, Periyasamy M, Dhakshinamoorthy V, Panneerselvam L, Perumal P (2017) Recurrent exposure to ferric oxide nanoparticles alters myocardial oxidative stress, apoptosis and necrotic markers in male mice. Chem Biol Interact 278:54–64

McShea (2007) Neuronal cell cycle re-entry mediates Alzheimer disease-type changes. Biochim Biophys Acta 1772(4):467–472. https://doi.org/10.1016/j.bbadis.2006.09.010

Meikrantz W, Schlegel R (1995) Apoptosis and the cell cycle. J Cell Biochem 58(2):160–174. https://doi.org/10.1002/jcb.240580205

Modi PK, Jaiswal S, Sharma P (2016) Regulation of neuronal cell cycle and apoptosis by MicroRNA 34a. Mol Cell Biol 36:84–94

Naser R, Vandenbosch R, Omais S, Hayek D, Jaafar C, Lafi SA, Saliba A, Baghdadi M, Skaf L, Ghanem N (2016) Role of the retinoblastoma protein, Rb, during adult neurogenesis in the olfactory bulb. Sci Rep 6(1). https://doi.org/10.1038/srep20230

Park DS, Morris EJ, Bremner R, Keramaris E, Padmanabhan J, Rosenbaum M, Shelanski ML, Geller HM, Greene LA (2000) Involvement of retinoblastoma family members and E2F/DP complexes in the death of neurons evoked by DNA damage. J Neurosci 20(9):3104–3114

Patil US, Adireddy S, Jaiswal A, Mandava S, Lee BR, Chrisey DB (2015) In vitro/in vivo toxicity evaluation and quantification of iron oxide nanoparticles. Int J Mol Sci 16(10):24417–24450. https://doi.org/10.3390/ijms161024417

Pelegrí C, Duran-Vilaregut J, del Valle J, Crespo-Biel N, Ferrer I, Pallàs M, Camins A, Vilaplana J (2008) Cell cycle activation in striatal

neurons from Huntington's disease patients and rats treated with 3-nitropropionic acid. Int J Dev Neurosci 26(7):665–671. https://doi.org/10.1016/j.ijdevneu.2008.07.016

Pucci B, Kasten M, Giordano A (2000) Cell cycle and apoptosis. Neoplasia 2:291–299

Schwartz EI, Smilenov LB, Price MA, Osredkar T, Baker RA, Ghosh S, Shi F, Vollmer TL, Lencinas A, Stearns DM, Gorospe M, Kruman II (2007) Cell cycle activation in postmitotic neurons is essential for DNA repair. Cell Cycle 6(3):318–329. https://doi.org/10.4161/cc.6.3.3752

Stone JG, Siedlak SL, Tabaton M, Hirano A, Castellani RJ, Santocanale C, Perry G, Smith MA, Zhu X, Lee H (2011) The cell cycle regulator phosphorylated retinoblastoma protein is associated with tau pathology in several tauopathies. J Neuropathol Exp Neur 70(7):578–587. https://doi.org/10.1097/NEN.0b013e3182204414

Sundarraj K, Raghunath A, Panneerselvam L, Perumal E (2017) Iron oxide nanoparticles modulate heat shock proteins and organ specific markers in mice male accessory organs. Toxicol Appl Pharmacol 317:12–24. https://doi.org/10.1016/j.taap.2017.01.002

Tahirbegi IB, Pardo WA, Alvira M, Mir M, Samitier J (2016) Amyloid Aβ 42 a promoter of magnetite nanoparticle formation in Alzheimer's disease. Nanotechnology 27(46):465102. https://doi.org/10.1088/0957-4484/27/46/465102

Thornton TM, Rincon M (2009) Non-classical P38 map kinase functions: cell cycle checkpoints and survival. Int J Biol Sci 5:44–52

Tyagi S, Herr W (2009) E2F1 mediates DNA damage and apoptosis through HCF1 and the MLL family of histone methyltransferases. EMBO J 28(20):3185–3195. https://doi.org/10.1038/emboj.2009.258

Vogel CF, Charrier JG, Wu D, McFall AS, Li W, Abid A, Kennedy IM, Anastasio C (2016) Physicochemical properties of iron oxide nanoparticles that contribute to cellular ROS-dependent signaling and acellular production of hydroxyl radical. Free Radic Res 50(11):1153–1164. https://doi.org/10.3109/10715762.2016.1152360

Wang B, Feng WY, Wang M, Shi JW, Zhang F, Ouyang H, Zhao YL, Chai ZF, Huang YY, Xie YN, Wang HF, Wang J (2007a) Transport of intranasally instilled fine Fe_2O_3 particles into the brain: microdistribution, chemical states, and histopathological observation. Biol Trace Elem Res 118(3):233–243. https://doi.org/10.1007/s12011-007-0028-6

Wang J, Zhoua G, Chena C, Yu H, Wang T, Mad Y, Jia G, Gao Y, Li B, Suna J, Li Y, Jiao F, Zhao Y, Chai Z (2007b) Acute toxicity and bio distribution of different sized titanium dioxide particles in mice after oral administration. J. Toxicol Lett 168(2):176–185. https://doi.org/10.1016/j.toxlet.2006.12.001

Wang W, Bu B, Xie M, Zhang M, Yu Z, Tao D (2009) Neural cell cycle dysregulation and central nervous system diseases. Prog Neurobiol 89(1):1–17. https://doi.org/10.1016/j.pneurobio.2009.01.007

Winer JL, Liu CY, Apuzzo ML (2012) The use of nanoparticles as contrast media in neuroimaging: a statement on toxicity. World Neurosurg 78(6):709–711. https://doi.org/10.1016/j.wneu.2011.08.013

Wu J, Ding T, Sun J (2013) Neurotoxic potential of iron oxide nanoparticles in the rat brain striatum and hippocampus. Neurotoxicology 34:243–253. https://doi.org/10.1016/j.neuro.2012.09.006

Yarjanli Z, Ghaedi K, Esmaeili A, Rahgozar S, Zarrabi A (2017) Iron oxide nanoparticles may damage to the neural tissue through iron accumulation, oxidative stress, and protein aggregation. BMC Neurosci 18:51–67

Zhang J, Herrup K (2008) Cdk5 and the non-catalytic arrest of the neuronal cell cycle. Cell Cycle 7(22):3487–3490. https://doi.org/10.4161/cc.7.22.7045

Zhang J, Li H, Zhou T, Zhou J, Herrup K (2012) Cdk5 levels oscillate during the neuronal cell cycle: Cdh1 ubiquitination triggers proteosome-dependent degradation during S-phase. J Biol Chem 287:25985–25994

Zhu (2007) Oxidative imbalance in Alzheimer's disease, apoptosis and the cell cycle. Mol Neurobiol 31:205–217